ELSEVIER

Journal of Alloys and Compounds 267 (1998) 79–85

Journal of ALLOYS AND COMPOUNDS

Crystal growth and structure of $Mn_{2.47}V_{0.94}Mo_{1.06}O_8$

Xiandong Wang, Kevin R. Heier, Charlotte L. Stern, Kenneth R. Poeppelmeier*

Department of Chemistry, Northwestern University, Evanston, IL 60208-3113, USA

Received 28 July 1997; received in revised form 14 October 1997

Abstract

Single crystals of $Mn_{2.47}V_{0.94}Mo_{1.06}O_8$ were grown in a $MnO/V_2O_5/MoO_3$ melt under a nitrogen atmosphere (orthorhombic, space group *Pnma* (No. 62), $a=5.167(2)$ Å, $b=10.580(3)$ Å, $c=17.868(4)$ Å, and $Z=6$). The crystallization, composition, and quality of the crystals were largely influenced by the composition of the melt, temperature and the oxygen partial pressure. © 1998 Elsevier Science S.A.

Keywords: $Mn_{2.47}V_{0.94}Mo_{1.06}O_8$; Structure; Crystal growth

1. Introduction

$Mg_{2.54}V_{1.08}Mo_{0.92}O_8$ [1] and $Zn_{3.77}V_{1.54}Mo_{1.46}O_{12}$ [2] have been discovered recently in the systems $MgMoO_4$–$Mg_3V_2O_8$ and $ZnMoO_4$–$Zn_3V_2O_8$, respectively. Owing to the similar sizes of the Mg^{2+}, Zn^{2+} and Mn^{2+} ions, $Mn_{2.5}VMoO_8$ was anticipated in the $MnMoO_4$–$Mn_3V_2O_8$ system. Manganese molybdate $MnMoO_4$ along with $CoMoO_4$, $NiMoO_4$ or $MgMoO_4$ exhibit good catalytic properties for the oxidative dehydrogenation of butane [3], and manganese orthovanadate $Mn_3V_2O_8$ [4], which is isostructural with $Mg_3V_2O_8$, may exhibit catalytic properties similar to $M_3V_2O_8$ (M=Mg, Zn, Ni and Cu) [5]. Similarly, mixed vanadium–molybdenum compounds may show unique catalytic properties.

Phase and structural information is important for understanding catalytic behavior and it is always useful to have single crystals to investigate the structures of new materials. In contrast to $Mg_{2.54}V_{1.08}Mo_{0.92}O_8$ and $Zn_{3.77}V_{1.54}Mo_{1.46}O_{12}$, the growth of $Mn_{2.5}VMoO_8$ single crystals can not be carried out in air, and the atmosphere used must be controlled to prevent the oxidation of Mn^{2+} and reduction of V^{5+} or Mo^{6+} during crystallization. Procedures for the growth of single crystals and the structure of the new compound $Mn_{2.5}VMoO_8$ are reported in this paper.

2. Experimental

2.1. Sample preparation

Polycrystalline $Mn_{2.5}VMoO_8$ was prepared by solid state reaction using MnO_2 (99.99%, Aldrich), V_2O_5 (≥99.6%, Aldrich) and MoO_3 (≥99.5%, Aldrich). After grinding in an agate mortar, the mixture was first calcined at 660°C for 5 h in air, then ground and pressed into pellets, and finally reacted at 900°C for 55 h in an oxygen-free nitrogen atmosphere (O_2 was removed at room temperature by MnO supported on silica) with one intermittent grinding. An XRD pattern of brown $Mn_{2.5}VMoO_8$ was recorded using Cu $K\alpha_1$ radiation (LiF monochromator, 2θ range of 15–100°, step scan: 0.02°/50 s, Si as internal standard) at 25°C. The melting point of polycrystalline $Mn_{2.5}VMoO_8$, as determined by Differential Thermal Analysis (TA Instruments Thermal Analyst 2000) in flowing nitrogen, was approximately 1013°C. In order to determine the existence of solid solutions and estimate the solubilities, a series of samples with nominal compositions $Mn_{2.5+x}V_{1+2x}Mo_{1-2x}O_8$ ($x=-0.15$ to 0.30) were prepared from Mn_2O_3 (99.9%, Aldrich), and the V_2O_5 and MoO_3 oxides previously described. The mixed powders were thoroughly ground and pressed into pellets, heated at 660°C for 12 h in air, then fired at 850°C for 12 h in flowing argon. After regrinding and repressing into pellets, the samples were finally heat treated at 900°C for 65 h in argon. For this series of samples, the XRD data were collected on a Rigaku X-ray diffractometer with Cu

*Corresponding author.

PII S0925-8388(97)00574-4

Kα radiation and nickel filter in the 2θ range of 15–75° (step scan: 0.05°/10 s, Si as internal standard) at 25°C. Polycrystalline $Mg_{2.5}VMoO_8$ and $Zn_{2.5}VMoO_8$ used for Thermogravimetric Analysis (TA Instruments Thermal Analyst 2000) were prepared in air at 1080°C and 800°C respectively.

$Mn_{2.47}V_{0.94}Mo_{1.06}O_8$ crystals were grown from the composition: 63 mol% MnO (99%, Aldrich), 18.5 mol% MoO_3 (≥99.5%, Aldrich) and 18.5 mol% V_2O_5 (≥99.6%, Aldrich) (composition #1 in Fig. 1). The mixture of oxides was heated to 1050°C at 120°C h^{-1}, held at 1050°C for 0.5 h, then cooled slowly to 880°C at 6°C h^{-1}, and finally cooled to room temperature at 60°C h^{-1}. Nitrogen gas flowed through the tube furnace at 25 cm^3 min^{-1} during the entire growth procedure. Residual O_2 in the nitrogen gas was removed at room temperature by MnO supported on silica, and further removed by MnO powder placed in the furnace immediately in front of the platinum boat containing the sample. The orange crystals obtained were thin rectangular bars (0.5–3 mm in length). The face perpendicular to the bar axis is the {100} plane, the other two faces are {010} and {001} respectively.

Vanadium-rich $Mn_{2.50}V_{1.30}Mo_{0.70}O_8$ crystals were grown from the composition: 72.22 mol% MnO, 5.56 mol% MoO_3 and 22.22 mol% V_2O_5 (composition #2) under an atmosphere of flowing O_2-free nitrogen. After heating to 1100°C, the melt was cooled to 900°C at 6°C h^{-1} followed by cooling to room temperature at 60°C h^{-1}. Red or brown needles crystallized on the surface of the melt.

Less vanadium-rich $Mn_{2.5+x}V_{1+2x}Mo_{1-2x}O_8$ ($0<x<0.166$) crystals were grown from composition: 66.66 mol% MnO, 16.67 mol% MoO_3 and 16.67 mol% V_2O_5 (composition #3). The cooling procedures and atmosphere are similar to the crystal growth conditions described above. A lower maximum temperature (T_{max}) of 1035°C was used for crystal growth (if $T_{max}\geq$1100°C, no crystals were obtained). Small dark brown crystals were obtained but they were not suitable for single crystal X-ray diffraction.

2.2. Determination of chemical composition

The crystal used for data collection was cut to expose a clean surface and analyzed by EDAX (Energy Dispersive Analysis of X-ray, Hitachi, Pioneer S-4500 SEM). The atomic ratio of Mn:V:Mo was determined to be 2.47:1.00:1.00 when a polycrystalline $Mn_{2.5}VMoO_8$ sample was used for calibration. The chemical composition of five batches of crystals were also analyzed by ICP-AES (Inductively Coupled Plasma Atomic Emission Spectrophotometry, Thermo Jarrell Ash, model Atomscan 25). Each sample was prepared by dissolving several clean crystals in dilute nitric acid. The average V:Mo composition was 0.94±0.02:1.06±0.02. Large uncertainty in the measurement of manganese by ICP prevented an accurate determination of the manganese content. Combining the EDAX and ICP results, the composition of the investigated crystal is approximately $Mn_{2.47}V_{0.94}Mo_{1.06}O_8$. The density of the polycrystalline $Mn_{2.5}VMoO_8$ powder 4.12(2) g cm^{-3} at 25°C [6] is in good agreement with the calculated density 4.22 g cm^{-3} at −120°C for $Mn_{2.47}V_{0.94}Mo_{1.06}O_8$.

The composition of the crystals grown at composition #2 was determined by EDAX only. Owing to their small size and poor crystallinity, the crystals grown from composition #3 were not analyzed.

2.3. Structure refinement

An orange and translucent $Mn_{2.47}V_{0.94}Mo_{1.06}O_8$ crystal with approximate dimensions of 0.32 mm×0.05 mm×0.02 mm was mounted on a glass fiber for study by single crystal X-ray diffraction. All measurements were made on an Enraf-Nonius CAD4 diffractometer with graphite monochromated Mo Kα radiation. Details of the structure determination and refinement are listed in Table 1. An analytical absorption correction [7] was applied which resulted in transmission factors ranging from 0.66 to 0.78. The data were corrected for Lorentz and polarization effects. A correction for secondary extinction was applied.

Table 1
Crystal data and details of $Mn_{2.47}V_{0.94}Mo_{1.06}O_8$ structure determination[a]

Chemical formula	$Mn_{2.47}V_{0.94}Mo_{1.06}O_8$
Formula weight	413.27
Crystal system	Orthorhombic
Space group	*Pnma* (No. 62)
a	5.167(2) Å
b	10.580(3) Å
c	17.868(4) Å
V	976.8(4) $Å^3$
Z	6
D_x, D_m [b]	4.22, 4.12(2) g cm^{-3}
μ (Mo Kα)	79.6 cm^{-1}
Crystal dimensions	0.32×0.05×0.02 mm^3
Radiation, wavelength	Mo Kα, 0.71069 Å
Temperature	−120.0°C
Scan type	$\omega-\theta$
Scan width	$(1.00+0.35\tan\theta)°$
$2\theta_{max}$	49.9°
No. of reflec. measured	total: 1877
	unique: 1377 (R_{int}=0.069)
No. of observations ($I>3.00\sigma(I)$)	731
No. of variables	56
Residuals: R[c], R_w [d,e]	0.047, 0.046
Goodness of fit	1.88
Final diff. Fourier peaks (max. min.)	1.45, −1.54 e $Å^{-3}$

[a] Further details of the crystal structure determination can be ordered from Fachinformationszentrum Karlsruhe, 76344 Eggenstein-Leopoldshafen, under the depository number CSD-No. 407760.
[b] Measured on $Mn_{2.5}VMoO_8$ powder.
[c] $R=\Sigma\|F_{obs}|-|F_{calc}\|/\Sigma|F_{obs}|$
[d] $R_w=[\Sigma w(|F_{obs}|-|F_{calc}|)^2/\Sigma w|F_{obs}|^2]^{1/2}$.
[e] $w=1/\sigma^2(F_{obs})$.

The observed systematic absences ($0kl$, $k+l=2n+1$; $hk0$, $h=2n+1$) are consistent with the space groups *Pnma* and $Pn2_1a$. The structure was solved by direct methods [8] and expanded using Fourier techniques [9], and refined satisfactorily in the centrosymmetric space group *Pnma*. The manganese atoms were refined anisotropically and all others isotropically. Vanadium and molybdenum atoms are statistically distributed on the two tetrahedral sites M(1) and M(2), and the manganese cation vacancies are localized on the Mn(2) site. This model is the same as the treatment for the $Mg_{2.54}V_{1.08}Mo_{0.92}O_8$ [1] and $Zn_{3.77}V_{1.54}Mo_{1.46}O_{12}$ [2] structures. The final cycle of full-matrix least-squares refinement converged with unweighted and weighted agreement factors: $R=0.047$ and $R_w=0.046$. Refinement on the population of Mn(2) resulted in a formula of $Mn_{2.50}V_{0.94}Mo_{1.06}O_8$ ($R=0.047$, $R_w=0.045$), which is in good agreement with the analyzed composition $Mn_{2.47}V_{0.94}Mo_{1.06}O_8$. Atomic positions, occupancies and thermal displacement parameters are presented in Table 2. Selected interatomic distances and bond angles are given in Table 3. All calculations were performed using the TEXSAN crystallographic software package of Molecular Structure Corporation [10].

2.4. Magnetic susceptibility

Magnetic susceptibilities of polycrystalline $Mn_{2.5}VMoO_8$ and $Mn_{2.47}V_{0.94}Mo_{1.06}O_8$ crystals were determined on a SQUID susceptometer (Quantum Design Corp., MPMS) between 5 and 300 K. About 23.1 mg $Mn_{2.5}VMoO_8$ powder and 8.8 mg orange/red crystals, encased in sealed gelatin capsules, were zero field cooled to 5 K. A 1 kG field was used for all measurements. The data were corrected for core diamagnetism using values from [11].

Table 3
Selected interatomic distances (Å) and bond angles (°) for $Mn_{2.47}V_{0.94}Mo_{1.06}O_8$

M(1)	–O(5)	1.77(1)	O(5)–M(1)–O(6)	108.8(4) (2×)
	–O(6)	1.753(9) (2×)	O(5)–M(1)–O(7)	114.6(6)
	–O(7)	1.73(1)	O(6)–M(1)–O(7)	109.4(4) (2×)
M(2)	–O(1)	1.782(9)	O(6)–M(1)–O(6)	105.5(6)
	–O(2)	1.726(9)	O(1)–M(2)–O(2)	110.9(4)
	–O(3)	1.760(8)	O(1)–M(2)–O(3)	104.9(4)
	–O4)	1.761(9)	O(1)–M(2)–O(4)	109.3(4)
Mn(1)	–O(3)	2.149(9)	O(2)–M(2)–O(3)	109.2(4)
	–O(3)	2.186(8)	O(2)–M(2)–O(4)	113.2(4)
	–O(4)	2.115(8)	O(3)–M(2)–O(4)	109.0(4)
	–O(5)	2.135(7)		
	–O(6)	2.128(9)		
	–O(6)	2.242(9)		
Mn(2)	–O(2)	2.11(1) (2×)		
	–O(2)	2.17(1) (2×)		
	–O(7)	2.18(1)		
	–O(7)	2.22(2)		
Mn(3)	–O(1)	2.153(9) (2×)		
	–O(1)	2.235(8) (2×)		
	–O(4)	2.135(9) (2×)		
Mn(2)	–Mn(2)	2.584(1)		

3. Results and discussion

The XRD pattern of $Mn_{2.5}VMoO_8$ powder is quite similar to that of $Mg_{2.5}VMoO_8$ [12]. The *d* values and relative intensities are given in Table 4. The calculated unit cell parameters are given in Table 5.

Only $MnMoO_4$ crystals were obtained from the starting composition $Mn_{2.5}VMoO_8$ indicating that $Mn_{2.5}VMoO_8$ melts incongruently, which is similar to $Mg_{2.5}VMoO_8$ in the $MgMoO_4$–$Mg_3V_2O_8$ system [1]. In contrast to the very good quality $Mg_{2.5}VMoO_8$ [1] and $Zn_{2.5}VMoO_8$ [2] crystals produced in earlier studies, only poorly crys-

Table 2
Atomic coordinates, occupation factors and temperature parameters for the $Mn_{2.47}V_{0.94}Mo_{1.06}O_8$ structure

Atom	Wyckoff position	*x*	*y*	*z*	Occ.	B_{iso} [a]/B_{eq} [b]
Mo(1)	4*c*	0.2204(5)	0.75	0.4435(1)	0.265	0.61(4)[a]
Mo(2)	8*d*	−0.2760(3)	0.4710(1)	0.34325(7)	0.530	0.65(3)[a]
V(1)	4*c*	0.2204(5)	0.75	0.4435(1)	0.235	0.61(4)[a]
V(2)	8*d*	−0.2760(3)	0.4710(1)	0.34325(7)	0.470	0.65(3)[a]
Mn(1)	8*d*	−0.2497(4)	0.5778(2)	0.52802(9)	1.0	0.82(4)[b]
Mn(2)	4*c*	−0.093(1)	0.75	0.2488(3)	0.3525	3.0(1)[b]
Mn(3)	4*c*	−0.7452(7)	0.25	0.3018(1)	0.5	0.91(5)[b]
O(1)	8*d*	−0.074(2)	0.3724(8)	0.2873(4)	1.0	0.9(2)[a]
O(2)	8*d*	−0.349(2)	0.6098(9)	0.2970(5)	1.0	1.6(2)[a]
O(3)	8*d*	−0.090(2)	0.5058(8)	0.4231(4)	1.0	0.7(2)[a]
O(4)	8*d*	−0.552(2)	0.3854(8)	0.3707(4)	1.0	0.6(2)[a]
O(5)	4*c*	−0.051(3)	0.75	0.5042(7)	0.5	1.0(2)[a]
O(6)	8*d*	0.413(2)	0.8819(8)	0.4639(4)	1.0	0.6(2)[a]
O(7)	4*c*	0.144(3)	0.75	0.3495(7)	0.5	1.3(3)[a]

[a] Isotropic refinement.

[b] $B_{eq}=\frac{8}{3}\pi^2(U_{11}(aa^*)^2+U_{22}(bb^*)^2+U_{33}(cc^*)^2+2U_{12}aa^*bb^*\cos\gamma+2U_{13}aa^*cc^*\cos\beta+2U_{23}bb^*cc^*\cos\alpha)$.

Table 4
Observed and calculated d_{hkl} (Å) values and observed relative intensities (I/I_0) for $Mn_{2.5}VMoO_8$ ($a=5.1783(3)$ Å, $b=10.5958(6)$ Å, $c=17.912(1)$ Å)

h	k	l	d_{hkl} – obs	d_{hkl} – cal[a]	I/I_0	h	k	l	d_{hkl} – obs	d_{hkl} – cal[a]	I/I_0
0	2	0	5.3017	5.2979	4	2	3	0	2.0880	2.0882	5
0	1	3	5.2025	5.2019	4	2	3	2	2.0342	2.0336	3
0	2	2	4.5563	4.5598	3	2	3	3	1.9713	1.9711	12
1	0	2	4.4829	4.4829	6	2	0	6	1.9558	1.9560	7
1	0	3	3.9119	3.9121	1	1	2	8	1.9163	1.9161	2
1	2	1	3.6273	3.6266	1	1	5	3	1.8640	1.8634	4
0	3	1	3.4647	3.4652	13	2	4	0	1.8516	1.8516	10
1	2	2	3.4211	3.4221	100	2	2	6	1.8349	1.8350	10
1	0	4	3.3876	3.3873	58	1	1	9	1.8287	1.8299	4
0	3	3	3.0404	3.0399	11	0	5	5	1.8235	1.8240	2
0	0	6	2.9847	2.9855	8	2	4	2	1.8139	1.8133	1
1	3	1	2.8799	2.8799	16	2	3	5	1.8043	1.8041	2
1	2	4	2.8535	2.8538	16	0	0	10	1.7919	1.7913	2
1	1	5	2.8377	2.8385	10	2	4	3	1.7673	1.7685	4
0	4	0	2.6492	2.6490	7	1	4	7	1.7340	1.7342	9
1	3	3	2.6217	2.6216	34	2	2	7	1.7212	1.7213	2
0	2	6	2.6002	2.6009	12	2	3	6	1.7114	1.7112	4
1	0	6	2.5869	2.5864	37	2	0	8	1.6937	1.6936	4
0	4	2	2.5388	2.5402	1	1	6	2	1.6433	1.6431	11
1	1	6	2.5129	2.5127	6	2	5	1	1.6331	1.6331	7
0	1	7	2.4879	2.4875	3	1	4	8	1.6238	1.6238	6
1	4	1	2.3389	2.3381	7	2	3	7	1.6173	1.6179	7
1	2	6	2.3236	2.3242	3	1	2	10	1.6125	1.6125	13
2	1	3	2.3173	2.3180	3	3	2	4	1.5405	1.5410	4
1	0	7	2.2946	2.2942	2	3	3	3	1.5013	1.5010	9
1	4	2	2.2803	2.2806	2	3	0	6	1.4943	1.4943	5
1	4	3	2.1938	2.1935	3	2	1	10	1.4594	1.4591	3
2	2	3	2.1678	2.1676	5	2	3	9	1.4408	1.4407	5
0	5	1	2.1039	2.1045	4						

[a] Calculated from POLSQ program, $\lambda = 1.54056$ Å.

tallized $Mn_{2.5+x}V_{1+2x}Mo_{1-2x}O_8$ crystals were grown from composition #3 (see Fig. 1) with $T_{max}=1035–1100$°C in O_2-free nitrogen. The smaller b and c axes calculated from powder X-ray diffraction of the $Mn_{2.5+x}V_{1+2x}Mo_{1-2x}O_8$ crystals (see Table 5), as compared with $Mn_{2.5}VMoO_8$ powder, indicate they are vanadium rich ($x>0$). Crystals ($Mn_{2.50}V_{1.30}Mo_{0.70}O_8$) grown from composition #2 have similar composition to the nominal composition #3 ($Mn_{2.667}V_{1.333}Mo_{0.667}O_8$) but are notably deficient in manganese. This reveals that the overall composition of the melt is probably too close to the solubility limit of $Mn_{2.5+x}V_{1+2x}Mo_{1-2x}O_8$ and too many nucleation centers are formed during cooling. A small weight loss (<1%) was also observed at this composition. This could easily bring the composition off the joining line between $Mn_{2.5}VMoO_8$ and $Mn_3V_2O_8$. To avoid the complexity along the joining line of $Mn_{2.5}VMoO_8$-$Mn_3V_2O_8$, and counter the evaporation of vanadium–molybdenum oxides, the composition was moved to the slightly more Mo–V-oxide rich composition #1, which lies on the joining line of the pseudo-binary of $Mn_{2.5}VMoO_8$ and $Mn_2V_2O_7$. Good quality $Mn_{2.47}V_{0.94}Mo_{1.06}O_8$ crystals could be grown repeatedly from this composition, although care must be taken to remove residual oxygen in the nitrogen during growth or dark brown crystals were formed. In summary, crystal growth of $Mn_{2.5}VMoO_8$ was most successful at composition #1 if the oxygen fugacity in the flowing inert gas was controlled such that Mn^{2+} is not oxidized and

Table 5
Cell parameters of $Mn_{2.5}VMoO_8$ powder and crystals with different compositions

	a (Å)	b (Å)	c (Å)	V (Å^3)	T(K)
$Mn_{2.5}VMoO_8$ [a]	5.1783(3)	10.5958(6)	17.912(1)	982.84(7)	298
$Mn_{2.5+x}V_{1+2x}Mo_{1-2x}O_8$ [b]	5.1782(9)	10.585(2)	17.859(2)	978.9(2)	298
$Mn_{2.47}V_{0.94}Mo_{1.06}O_8$ [c]	5.167(2)	10.580(3)	17.868(4)	976.8(4)	153
$Mn_{2.50}V_{1.30}Mo_{0.70}O_8$ [d]	5.172(4)	10.549(3)	17.856(4)	975.7(4)	153

[a] Powder prepared at 900°C in O_2-free N_2.
[b] Crystal grown from composition #3 (Fig. 1), $x>0$.
[c] Crystal from composition #1.
[d] Crystal from composition #2.

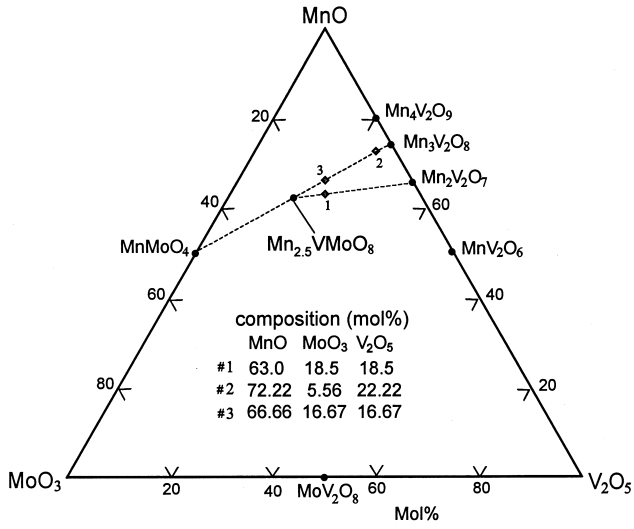

Fig. 1. Compositions used for the crystal growth of $Mn_{2.5}VMoO_8$ are shown in the ternary system $MnO–MoO_3–V_2O_5$.

V^{5+}/Mo^{6+} are not reduced at the crystallization temperatures.

$Mn_{2.47}V_{0.94}Mo_{1.06}O_8$ is isostructural with $Mg_{2.54}V_{1.08}Mo_{0.92}O_8$ and closely related to $Zn_{3.77}V_{1.54}Mo_{1.46}O_{12}$ (see Fig. 2). $Mn(1)O_6$ octahedra share corners and edges with their neighbors and form zig-zag planes perpendicular to the *c* direction. The face-shared $Mn(2)O_6$ octahedral chains are parallel to the *a* direction. The unusual $Mn(3)O_6$ trigonal prisms share edges and form columns parallel to the *a* axis. The various types of MnO_6 polyhedra are linked by the $(V/Mo)O_4$ tetrahedra to form the three-dimensional network. The extremely short Mn(2)–Mn(2) distance (2.584 Å) is shorter than the Mn–Mn distance in manganese metal (2.668 Å) [13].

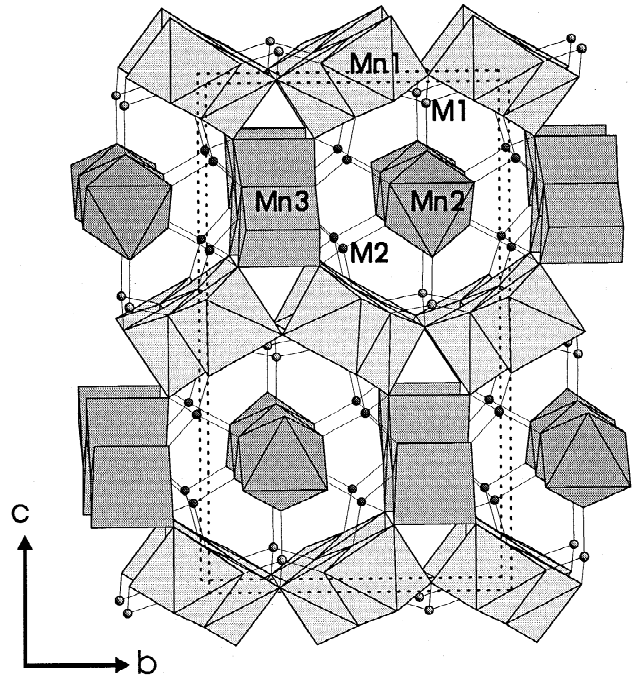

Fig. 2. Structure of $Mn_{2.47}V_{0.94}Mo_{1.06}O_8$ viewed approximately along the *a* axis. Metal–oxygen polyhedra are labelled. M1 and M2 stand for disordered vanadium and molybdenum (V/Mo).

In contrast to the coexistence of Co^{2+} and Co^{3+} in isostructural $NaCo_{2.31}(MoO_4)_3$ [14], bond valence calculations [15] suggest that all three types of manganese ions exist as Mn^{2+} (Table 6), This agrees with the proposed formula, $Mn_{2.47}V_{0.94}Mo_{1.06}O_8$, in which vanadium and molybdenum hold their highest oxidation states (V^{5+} and Mo^{6+}). Mn–O bond lengths vary within 2.11–2.24 Å (Δ=0.13 Å) for all MnO_6 polyhedra, very similar to Mg–O bond length variation 2.03–2.17 Å (Δ=0.14 Å) in $Mg_{2.5}4V_{1.08}Mo_{0.92}O_8$ but less than Zn–O bond length variation 2.01–2.44 Å (Δ=0.43 Å) in $Zn_{3.77}V_{1.54}Mo_{1.46}O_{12}$. The large Δ value of Zn–O bonds is caused by distortion of the trigonal prismatic ZnO_6. As a result, $Mn_{2.47}V_{0.94}Mo_{1.06}O_8$ and $Mg_{2.5}4V_{1.08}Mo_{0.92}O_8$ have the same space group, *Pnma*, while $Zn_{3.77}V_{1.54}Mo_{1.46}O_{12}$ has a different space group, $P2_12_12_1$, as discussed in [2]. The unusual MnO_6 trigonal prisms also exist in Mn_2GeO_4 [17] and $Mn_5(PO_4)_3Cl_{0.9}(OH)_{0.1}$ [18].

For the series $M_{2.5+x}V_{1+2x}Mo_{1-2x}O_8$ ($M=Mg^{2+}$, Zn^{2+} and Mn^{2+}) we observed that when the size of the M^{2+} ion increases ($r(Mg^{2+})<r(Zn^{2+})<r(Mn^{2+})$), the occupancy of the face-shared octahedral sites ($Occ(Mg^{2+})$=81%, $Occ(Zn^{2+})$=77%, $Occ(Mn^{2+})$=70%) and the vanadium content decrease. That is, in the case of Mn^{2+} the compound becomes Mo rich, while the smaller Mg^{2+} and Zn^{2+} cations result in V rich compounds. This trend is followed as long as M^{n+} remains divalent. The high vanadium phase $Mn_{2.50}V_{1.30}Mo_{0.70}O_8$ has the same structure as $Mn_{2.47}V_{0.94}Mo_{1.06}O_8$, but the charge is not compensated for by adding more Mn^{2+} to the octahedral chain sites. Rather, Mn^{2+} is partially oxidized to balance the overall charge and the average oxidation state of manganese is +2.12. This interesting solid state redox chemistry can not occur in the $Mg_{2.5+x}V_{1+2x}Mo_{1-2x}O_8$ and $Zn_{2.5+x}V_{1+2x}Mo_{1-2x}O_8$ systems.

The cell parameters of $Mn_{2.50}V_{1.30}Mo_{0.70}O_8$ and $Mn_{2.47}V_{0.94}Mo_{1.06}O_8$ (Table 5) reveal that an increase in the V/Mo ratio causes the *b* and *c* axes to contract significantly while the *a* axis expands slightly. The same tendency was found in the solid solution

Table 6
Manganese bond valence calculated by $\nu=\Sigma\exp[(R_0-R)/0.37]$ [15] for $Mn_{2.47}V_{0.94}Mo_{1.06}O_8$, as compared with $Mn_3V_2O_8$ and $MnMoO_4$

Compound	Bond valence				Ref.
	Mn(1)	Mn(2)	Mn(3)	Average	
$Mn_{2.47}V_{0.94}Mo_{1.06}O_8$	2.22	2.22	2.14	2.19	This work
$Mn_3V_2O_8$	2.07	2.17		2.12	[4]
$MnMoO_4$	2.20	2.21		2.21	[16]

$Mg_{2.5+x}V_{1+2x}Mo_{1-2x}O_8$ [1]. By calculating the cell parameters of the polycrystalline samples treated at 900°C in argon atmosphere, the vanadium and molybdenum solubilities of $Mn_{2.5x}V_{1+2x}Mo_{1-2x}O_8$ ($-0.05 \leq x \leq 0.15$) were estimated (Fig. 3). The V:Mo ratio in the vanadium rich solid solution limit $\approx Mn_{2.65}V_{1.30}Mo_{0.70}O_8$ is consistent with the $Mn_{2.50}V_{1.30}Mo_{0.70}O_8$ crystals.

The reciprocal magnetic susceptibilities versus temperature for $Mn_{2.5}VMoO_8$ powder and $Mn_{2.47}V_{0.94}Mo_{1.06}O_8$ crystals are presented in Fig. 4. The powder and crystal samples have essentially the same magnetic properties. Both display Curie–Weiss paramagnetic behavior [19] in the high temperature range. A least squares fitting of the data for the $Mn_{2.5}VMoO_8$ powder between 50 and 300 K gave a Curie constant $C=4.75$ emu K (Mn mol)$^{-1}$, which corresponds to an effective moment $\mu_{eff}=6.21$ μ_B/Mn atom, and Weiss constant $\theta=-210$ K. Data from the crystal sample gave a Curie constant $C=4.99$ emu K (Mn mol)$^{-1}$, which corresponds to an effective moment $\mu_{eff}=6.37$ μ_B/Mn atom, and Weiss constant $\theta=-210$ K. Comparing with the value 5.92 μ_B expected for the high spin-only Mn^{2+} ion [20], it is believed that all manganese ions exist in the high spin Mn^{2+} state, which is consistent with the composition analysis and bond valence calculations. The negative Weiss constants indicate the dominant interactions between Mn^{2+} ions are antiferromagnetic.

It was noted that these curves are convex upward in the low temperature range ($5\ K \leq T \leq 50$ K), and the effective magnetic moment calculated is higher than that for spin-only Mn^{2+} ions. Owing to the complex magnetic interactions that take place in the three-dimensional network of $Mn(1)O_6$ octahedra and $Mn(3)O_6$ trigonal prisms, and one-dimensional chains of $Mn(2)O_6$ faced-shared octahedra, it is difficult to find a proper model to satisfactorily describe the experimental $1/\chi \sim T$ curve. However, the contribution to the above two features from MnO_6 clusters in the faced-shared octahedral chains (if manganese atoms are randomly distributed within a chain, the average length of a manganese atom chain Mn_n corresponds to $n=3.39$) may play a dominant role. Similar behavior of $1/\chi \sim T$ was observed in $V_{1.23}(PO_4)(OH)_{0.69}(H_2O)_{0.31}\cdot 0.33H_2O$ owing to antiferromagnetic exchange coupling between the vanadium cations in the face-sharing vanadium–oxygen octahedral chains [21]. The magnetic interactions of the dominant species (face-shared MnO_6 trimers) may be similar to the face-shared VO_6 dimers, but the former will be more complex than the latter.

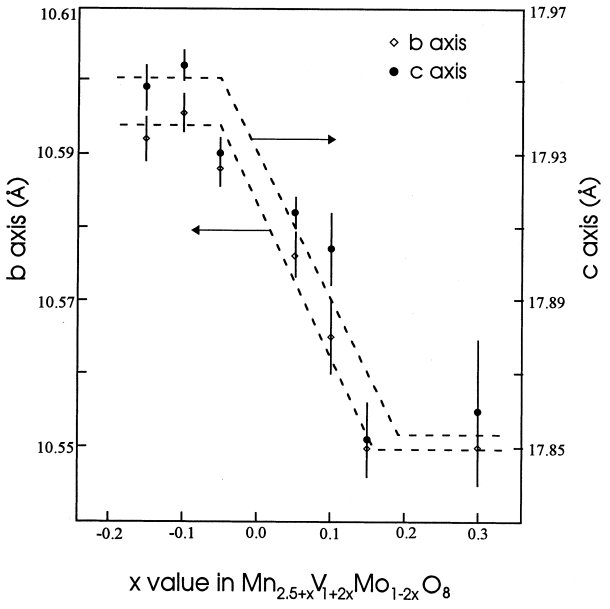

Fig. 3. Lattice parameters b and c of $Mn_{2.5+x}V_{1+2x}Mo_{1-2x}O_8$ as a function of nominal composition.

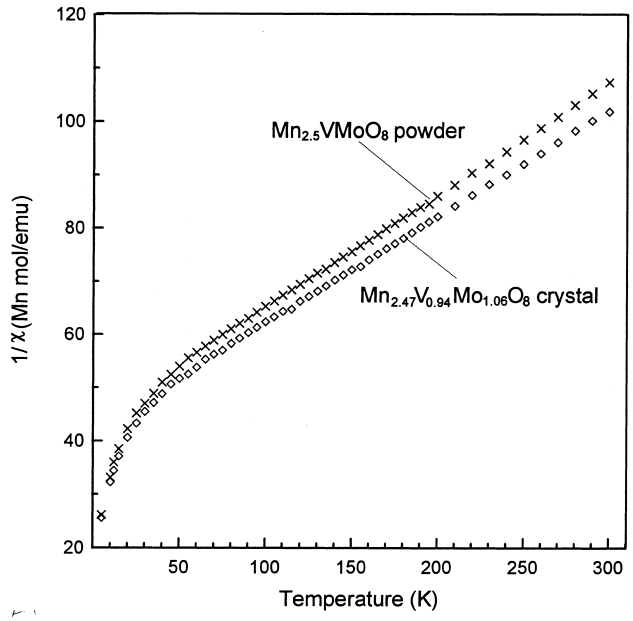

Fig. 4. Plots of reciprocal molar magnetic susceptibilities versus temperature from 5 to 300 K for $Mn_{2.5}VMoO_8$ powder and $Mn_{2.47}V_{0.94}Mo_{1.06}O_8$ crystals.

The reduction of polycrystalline $M_{2.5}VMoO_8$ (M=Mn, Mg and Zn) powders in 7% H_2 in nitrogen (Fig. 5) revealed that the reducibilities are in the order of '$Mg_{2.5}$' ($T_{onset}=777$°C)>'$Mn_{2.5}$' ($T_{onset}=660$°C)>'$Zn_{2.5}$' ($T_{onset}=534$°C) and unlike the zinc and magnesium analogues $Mn_{2.5}VMoO_8$ can be oxidized in air at about 300°C. A weight gain of approximately 2.8% was observed after heat treatment at 800°C for 5 h. These oxidation-reduction properties could be interesting for catalytic reactions.

4. Conclusions

Good quality $Mn_{2.47}V_{0.94}Mo_{1.06}O_8$ crystals were obtained under specific conditions of composition and inert atmosphere. The compound is isostructural with $NaCo_{2.31}(MoO_4)_3$, $Mg_{2.54}V_{1.08}Mo_{0.92}O_8$ and $(Cu,Mn)_{3.66}Mo_3O_{12}$ [22]. Within the structure, all man-

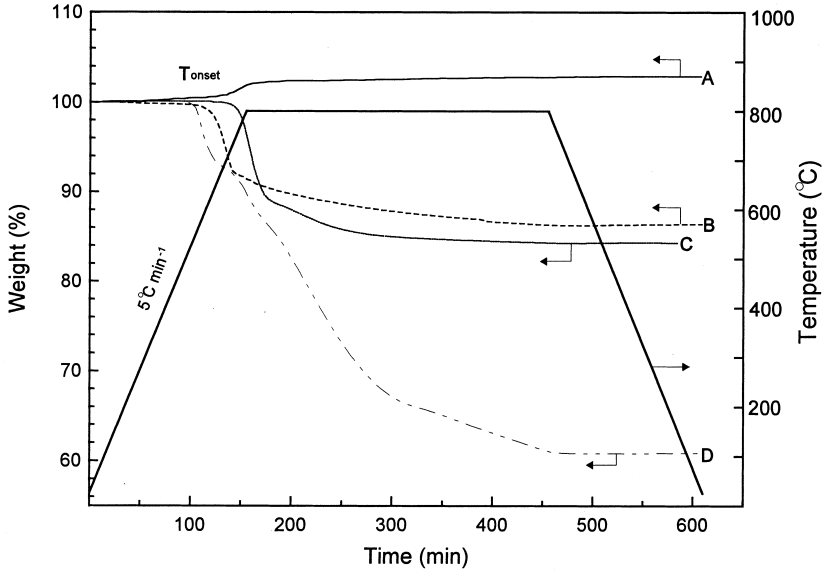

Fig. 5. Thermogravimetric analysis for the oxidation of $Mn_{2.5}VMoO_8$ (A) in air (flow-rate: 20 $cm^3\,min^{-1}$) and the reduction of polycrystalline $Mn_{2.5}VMoO_8$ (B), $Mg_{2.5}VMoO_8$ (C) and $Zn_{2.5}VMoO_8$ (D) in 7% H_2 in N_2 (flow-rate: 20 $cm^3\,min^{-1}$).

ganese ions preserve their low oxidation state (Mn^{2+}) while vanadium and molybdenum remain in their highest oxidation states (V^{5+} and Mo^{6+}). This feature and the Mn^{2+} cation vacancies may give the material interesting catalytic properties. The phase relationships in the ternary system $MnO–MoO_3–V_2O_5$ are under investigation.

Acknowledgements

The authors wish to thank Dr. Larry Cirjak and acknowledge an Extramural Research Award (EMRA) from BP America, Inc., the National Science Foundation (NSF) (No. DMR-9412971) and the Materials Research Center of Northwestern University supported by NSF (DMR-9632472) for support of this work.

References

[1] X.D. Wang, C.L. Stern, K.R. Poeppelmeier, J. Alloys Comp. 243 (1996) 51.
[2] X.D. Wang, K.R. Heier, C.L. Stern, K.R. Poeppelmeier, J. Alloys Comp. 255 (1997) 190.
[3] D.N. Tmenov, L.P. Shapovalova, V.I. Voznyuk, V.A. Doroshenko, V.P. Luk'yanenko, Khim Prom-st. (Moscow) 12 (1986) 741.
[4] X.D. Wang, C.L. Stern and K.R. Poeppelmeier, in preparation.
[5] O.S. Owen, H.H. Kung, J. Mol. Catal. 79 (1993) 265.
[6] M.Y. Chern, R.D. Mariani, D.A. Vennos, F.J. DiSalvo, Rev. Sci. Instrum. 61 (1990) 1773.
[7] J. de Meulenaer, H. Tompa, Acta Crystallogr. 19 (1965) 1014.
[8] G.M. Sheldrick, SHELX86, in: G.M. Sheldrick, C. Kruger, R. Goddard (Eds), Crystallographic Computing 3, Oxford University Press, 1985, p. 175.
[9] P.T. Beurskens, G. Admiraal, G. Beurskens, W.P. Bosman, S. Garcia-Granda, R.O. Gould, J.M.M. Smits, C. Smykalla, DIRDIF92, in: The DIRDIF Program System, Technical Report of the Crystallography Laboratory, University of Nijmegen, The Netherlands, 1992.
[10] TEXSAN-TEXRAY Structure Analysis Package Molecular Structure Corporation, 1985.
[11] L.N. Mulay, in: Magnetic Susceptibility, John Wiley and Sons, New York, 1963, p. 1782.
[12] V.G. Zubkov, I.A. Leonidov, K.R. Poeppelmeier, V.L. Kozhevnikov, J. Solid State Chem. 111 (1994) 197.
[13] W.B. Pearson (Ed.), in: A Handbook of Lattice Spacings and Structures of Metals and Alloys, Pergamon Press, vol. 2, 1967, p. 85.
[14] J.A. Ibers, G.W. Smith, Acta Crystallogr. 17 (1964) 190.
[15] I.D. Brown, D. Altermatt, Acta Crystallogr. B41 (1985) 244.
[16] S.C. Abrahams, J.M. Reddy, J. Chem. Phys. 43 (1965) 2533.
[17] N. Morimoto, M. Tokonami, K. Koto, S. Nakajima, American Mineral. 57 (1972) 62.
[18] G. Engel, J. Pretzsch, V. Gramlich, W.H. Baur, Acta Crystallogr. B31 (1975) 1854.
[19] L.N. Mulay, Magnetic Susceptibility, Interscience Publishers, 1963, p. 1772.
[20] B. Lippold, J. Herrmann, W. Reichelt, H. Oppermann, Phys. Stat. Solidi K59 (1991) 124.
[21] J.T. Vaughey, W.T.A. Harrison, A.J. Jacobson, D.P. Goshorn, J.W. Johnson, Inorg. Chem. 33 (1994) 2481.
[22] O. Sedello, Hk. Müller-Buschbaum, Z. Naturforsch. 51B (1996) 447.